Probing the electronic structure of buried interfaces via resonant scattering methods

Zachary Porter

Stanford Synchrotron Radiation Lightsource,

2575 Sand Hill Road, MS 99, Menlo Park, California 94025, USA

(Dated: August 20, 2015)

Devices such as next-generation magnetic read heads demand energy storage capabilities and switching times beyond what is met by current permanent magnets. Superlattices of soft and hard ferromagnets (FM) that exhibit exchange-spring coupling are well-suited to be optimized for this purpose. Because of perovskites' tunable properties from competing charge and spin degrees of freedom, one such system of interest is (001)-oriented $La_{0.7}Sr_{0.3}CoO_3$ (LSCO) capped with $La_{0.7}Sr_{0.3}MnO_3$ (LSMO). In the interfacial layers, FM moments are exchange-coupled strongly to each other, increasing overall coercivity. However, this system has subtleties that cannot be teased out in simple spin orientation models. In particular, growth mechanisms lead to rough interfaces and interlayer diffusion, which may drive a poorly understood phenomenon. The LSCO interfaces exhibit distinct magnetic properties from the bulk, possibly owing to an unexpected Co^{2+} oxidation state near the LSMO that could lead to superexchange with Mn^{4+} or possibly antiferromagnetism. Therefore the characterization of the electronic structure of interfaces is crucial to our understanding of the magnetic structure, but this is impossible with surface techniques, since most interfaces are buried, as well as spectroscopy, because the layers are similar in density. Specular x-ray reflectivity (SXR) is one method that describes layer thickness, density, and out-of-plane interface roughness of surfaces and buried interfaces. To characterize further, we apply SXR over absorption edges to increase Co/Mn contrast. Back-conversion to x-ray absorption near-edge structure (XANES) provides spectroscopic information on oxidation states that considers each sublayer separately, thereby determining how the sublayers couple.

I. INTRODUCTION

Exchange-spring coupling is an emergent phenomenon similar to the exchange bias in antiferromagnetic/ferromagnetic (AFM/FM) interfaces: the hard layer pins the soft layer's magnetic moments. The resulting combination the has best traits of each layer: large coercivity as well as high saturation magnetization [1]. This boosts the energy stored by the magnet, because it is proportional to the integral of the magnetic hysteresis loop[2], $U = \int M\, dH$.

Prior results from -ray magnetic circular dichroism (XMCD) spectroscopy indicate that different magnetic states are visible in LSCO/LSMO bilayer interfaces compared to the

This material is based upon work supported by the U.S. Department of Energy, Office of Science, Office of Workforce Development for Teachers and Scientists (WDTS) under the Science Undergraduate Laboratory Internship (SULI) program, under Contract No. DE-AC02-76SF00515.

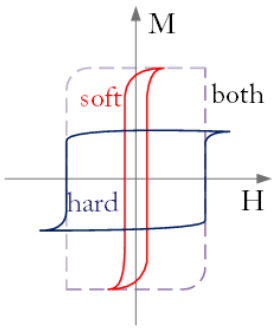

FIG. 1. The magnetic hysteresis loop for an FM exchange-spring system.

bulk layers[1]. In the bulk the LSCO is ferromagnetic under ambient conditions in thin films for the $x = 0.3$ strontium doping in this sample; it is stably FM in the range $0.2 \leq x \leq 0.5$ due to double exchange[3] between Co^{3+} and Co^{4+}. The collaborators indicated in previous publications that they suspect that the LSCO interfacial layer with the substrate is in a low-spin "non-magnetic" state for 4nm (∼10 unit cells) due to strain-induced lattice mismatch. Most interestingly, the direct exchange between like ions is expected to cause AFM coupling [3] at the LSCO/LSMO interface.

In order to characterize these magnetic states, it is necessary to determine the oxidation states of the B transition metal ions in the ABO_3 perovskite lattices that mediate the exchange interactions. Absorption spectroscopy (e.g. XANES), which contains this information and a wide array of additional electronic information [4], imposes a spectroscopic average over bulk and interfacial layers, so scattering is necessary for examining the buried interfaces. Examining resonant energies in specular x-ray reflectivity (SXR) is necessary to improve contrast amongst similar layers, and also can be fitted and subsequently transformed to yield XANES-like data for the individual layers.

This analysis is important because LSCO is riddled with growth difficulties such as ordered oxygen vacancies which may be tuned slightly to induce changes in structure [5]. Unfortunately, strain can preferentially change the direction of the O vacancies, making it hard to discern whether LSCO's magnetic properties are intrinsic or result from specific growth conditions. Another complication is that imperfect interfaces make exchange coupling along different orientations energetically favorable, canting the spin axis and yielding different magnetic structure [6]. It is difficult to account for these growth difficulties, but by careful resonant SXR fitting one may get closer to accurately refining the structure and chemistry intrinsic to this material.

Resonant SXR is just one tool for interface characterization. In order to develop a defensible structural model, I suggest diffraction for verifying lattice parameters and shape. In addition, off-specular (or diffuse) reflectivity (OSXR) and crystal truncation rods (CTR) are important measurements for buried interface structure. A qualitative analysis of OSXR can show the extent to which the roughness of the layers is correlated [7][8], and quantitative analysis gives in-plane roughness and interlayer diffusion[9][10], which SXR lacks. Exchange mechanisms are

sensitive to bond angle changes (and competing mechanisms in the LSMO sublayer) and thus CTR, which can describe 2D crystallography at interfaces[11], would also aid this characterization effort.

I present my findings from a resonant SXR study for sample X11, comprised of a $(LaAlO_3)_{0.3}(Sr_2AlTaO_6)_{0.7}$ (LSAT) substrate, 12nm of LSCO, and 6nm of LSMO, all in the (001) orientation. This sample was grown via pulsed laser deposition by Binzhi Li, a graduate student in Yayoi Takamura's group at the University of California, Davis. The novelty of this paper is that the LSCO interfaces are modeled as distinct from the bulk. In parallel with complementary measurements, I arrive at an improved method for characterizing interfaces of complicated lattices, with superior functionality and performance over more conventional permanent magnets in devices.

II. DATA COLLECTION

Data on sample X11 was collected on the week of August 3, 2015 at Beamline 2-1. I cleaned the sample in isopropyl alcohol and deionized water, sonicating for 2 minutes in each, directly prior to measurements and placed it in the He-filled sample chamber over a small vacuum to hold it in place. First I aligned the sample in the beam using SPEC© software by measuring with the ion chamber, and adjusted slits to get the desired beam size for my sample size (in this case, 65μm). Next I took initial XANES, using a VORTEX® silicon drift x-ray detector aligned perpendicular to the beam direction to examine fluorescence, by stepping in energy around the Mn and Co edges.

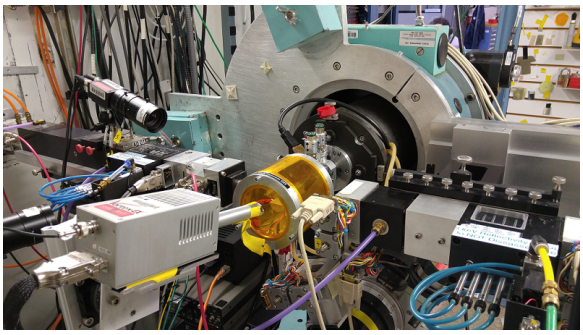

FIG. 2. The experimental setup on Beamline 2-1 at SSRL. The detector for fluorescence is visible (bottom-left), perpendicular to the sample.

Then I took SXR with another VORTEX® detector located at 2θ, the specularly reflected angle from the beam, by stepping in θ but with linearly increasing detection times. This helped increase photon counts at higher angles, decreasing our statistical uncertainty. In order to get the background photon counts, which are subtracted out at each energy, I repeated this scan at off-specular angles ($2\theta = 2 \times \theta - 0.5°$). I repeated this at energies near the absorption edge, and at non-resonant energies far from edges for comparison. I needed filter boxes to protect the detectors, and calibrated them for a wide incident energy range.

In the future, these results may be augmented by OSXR information. In July, I used this on a

previous sample called ZQL4, which had alternating 18 unit cell sublayers of LSMO and LSFO ($La_{0.7}Sr_{0.3}FeO_3$), repeated five times. I took OSXR by repeatedly performing "background" scans around various 2θ values. I did not perform this measurement on X11 because the compiled OSXR curves, known as "Resonant Diffuse Scattering" or "banana" plots, seemed difficult to analyze quantitatively. Qualitatively they had no curved horizontal lines (bananas), revealing that for ZQL4 the in-plane roughness was uncorrelated (see Figure 3 below), but I lacked sufficient beam time to examine X11.

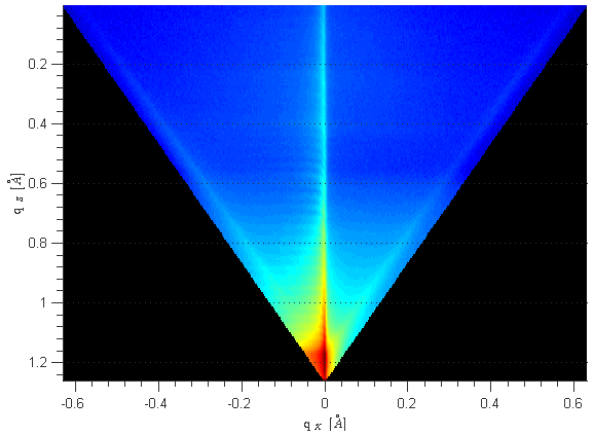

FIG. 3. Resonant Diffuse Scattering (logarithmic intensity heatmap, red is high, [a.u.]) at 10keV for ZQL4, an LSMO/LSFO superlattice grown on (111) $SrTiO_3$.

III. RESONANT SXR THEORY

Scattering theory begins with a consideration of refraction from the layers of the material comprising a sample. Index of refraction typically lies slightly below 1 (by $\approx 10^{-5}$) for x-rays in materials, to account for x-rays bending toward interfaces. While this looks worrisome at first glance, since $n = c/v$ which seems to imply that the speed of light exceeds c, in this case v is the phase velocity and not the group velocity. Also, due to absorption, there is a tiny imaginary component to n. These differences in n from unity are denoted as $n = 1 - \delta + i\beta$. We use δ and β, which are known for the elements, to calculate reflectivity, as we will see in the subsequent section, for multiple scattering on multi-layered films. Luckily, there is a secondary definition that starts from treating electrons on the constituent atoms of a molecule as scatterers to get at n [12]:

$$n = 1 - \frac{2\pi\rho_{at}r_0}{k^2} f(Q, E), \qquad (1)$$

where ρ_{at} is the atomic electron density, r_0 is the Thomson scattering length, $k{=}|\vec{k}_{inc}|$ is the incident wavevector's magnitude, $Q = \vec{k}_{inc} - \vec{k}_{ref} = 2k\sin\theta$ in $[\mathring{A}^{-1}]$ is the (elastic) wavevector transfer or scattering vector, and $E{=}ck$ is incident photon energy. Of most interest here is the atomic scattering length:

$$f(Q, E) = f_0(Q) + f'(E) + if''(E), \qquad (2)$$

separated here into constant (in energy), real, and imaginary components. The constant factor $f_0(Q{=}0) \approx Z$, the atomic number, if we neglect a small relativistic correction at high E, and note that, in reflectivity, $Q{\sim}0$ to good approximation. This alternative definition of n is useful because,

as a result of electromagnetic waves being analytic on the complex plane, they are causal, and one may relate $f'(E)$ and $f''(E)$. Their relation is called the K-K Transform, and is discussed in Section V along with the interpretation of f'' as XANES, which is rich in electronic information.

In order to simulate the sample, we need to go between the indices of refraction of the layers and the SXR data. To accomplish this, the Parratt function uses fit parameters for the layers to simulate scattering off of the sample. Each layer is modeled by a characteristic thickness $t[\mathring{A}]$, out-of-plane surface roughness $\sigma[\mathring{A}]$, density $d[1/\mathring{A}^3]$, and complex scattering length $f = (f_0 + f') + i(f'')$, $[a.u.]$ [1]. The density and scattering length are somewhat redundant, so to avoid overdefining the sample one must be left constant. In this work I fit the real and imaginary parts of scattering length and leave density as the theoretical volume of the unit cell.

In this regime, these parameters are used to find the real and imaginary parts of index of refraction (δ and β), at height z. To check if the electron densities and roughnesses are physical, these may be inspected graphically. They are comparable to the real and imaginary parts of the SLD (scattering length density, $[r_0/\mathring{A}^3]$) graph used in similar programs like GenX[13] (see Figure 4).

From here the program calls the Parratt function, an exact recursive method that generalizes Fresnel's equations for multilayers, to calculate the reflection intensity. The current algorithm was developed by Trevor Petach, and it calculates δ and β at regularly spaced height values, using error functions $\sum_{i\ interfaces} erf(z - z_i)$ to estimate interfaces. This method is more computationally intensive than another method, called Nevot-Croce, which treats δ and β as continuous. Use of this function would save an estimated order on magnitude of CPU time per calculation.

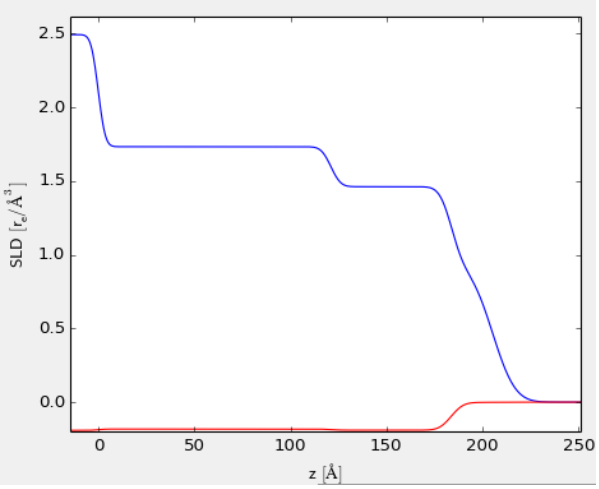

FIG. 4. An SLD for sample X11 at the Mn edge, from GenX[13], which uses Nevot-Croce. Real is blue, imaginary is red.

SXR is always plotted as $log(I)$ vs. Q when comparing results from multiple energies. Intensity I is a count of the number of photons at the incident energy range of interest, normalized by the monitor to be consistent when changing time steps. In the Parratt formalism, thickness manifests as the period of interference oscillations, roughness makes log(intensity) die

[1] Also, SXR is sensitive to host of additional instrumental parameters, because scattering is ultimately a convolution of the beam with the sample.

off faster, and density or scattering length modifies the intensity difference between interference peaks (known as Kiessig fringes). The critical angle, as a general observation, is mostly a result of the top layer's density, though it is a function of energy as well.

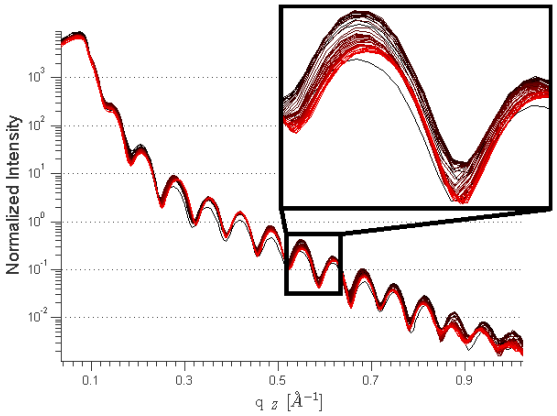

FIG. 5. SXR for X11, over a wide energy range centered about the Co K_β edge. Energy is increasing from red to black.

IV. FITTING WITH GENETIC ALGORITHMS

The overall strategy for fitting SXR data for samples with low layer contrast is as follows:

First, roughly fit a dataset at a nonresonant energy to determine instrumental parameters and get a starting point on layer parameters.

Second, fit a resonant dataset at some element's absorption edge (in this case Mn) to verify the layer properties, including the interlayer roughness, which is not observable at nonresonant energies.

Lastly, fit resonant datasets at energies along the absorption edge of the element under examination (in this case Co), fitting with the fewest number of parameters besides $f'(E)$ and $f''(E)$ to isolate the electronic changes.

I developed an algorithm to accomplish the last step above so that I would have finer control over the fits using the Matlab® Optimization Toolbox^{TM}. The fitting routine is a genetic algorithm (GA), which has distinct merits over most algorithms when there are many parameters to fit and many objective functions to satisfy. In order to quantify the appropriateness of the fits, and to pick the right energies for the data to examine, I use the methods in the proceeding subsections.

I compare the calculated reflection intensity I_c to I_m, the measured reflectivity scans from Beamline 2-1 at the Stanford Synchrotron Radiation Lightsource (SSRL), using a statistical test called figure of merit, abbreviated FOM. This is a standard test for fits that favors agreement to measurement as well as simple models, because it weights with input parameters. In this project, I chose the figure of merit formula from a similar program called GenX [13]:

$$FOM = \frac{1}{N-p} \sum_i \left| ln\Big(I_c(i)\Big) - ln\Big(I_m(i)\Big) \right| \quad (3)$$

where we define n as one data point (observation in theta or q-space), N as the total number of data points, and p is the number of parameters. It is important to subtract the background from the measured intensities I_m because it is

impossible to account for this accurately as a fit parameter.

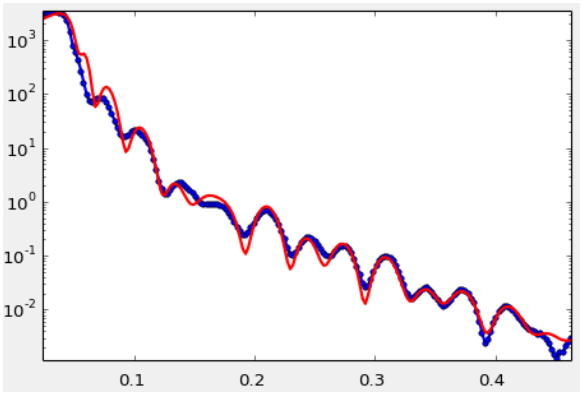

FIG. 6. An SXR fit (log(I) vs. Q) for sample X11 at the Mn edge, from GenX[13]. Blue is measured, red is the simulation. Note the poor fit (FOM=0.11), resulting from a poor physical model. The table values for f' at resonant energies are inexact, and there is likely a missing layer.

V. K-K TRANSFORMS

The relations between $f'(E)$ and $f''(E)$ follow from a consideration of electrons as damped harmonic oscillators. For the derivation, which is helpful to understanding the utility of the equations, see Appendix A. The useful form of the relations, known as the Kramers-Kronig (K-K) transforms, is, evaluated at E_0 [14]:

$$f'(E_0) = \frac{2}{\pi} \mathcal{P}\int_0^\infty \frac{E f''(E)}{E^2 - E_0^2}\, dE \qquad (4)$$

$$f''(E_0) = -\frac{2E_0}{\pi} \mathcal{P}\int_0^\infty \frac{f'(E)}{E^2 - E_0^2}\, dE \qquad (5)$$

These formulas are easy to implement, in principle. But in practice, tabulated values are difficult to deal with. The NIST tables, used in this work, were obtained from self-consistent Dirac-Hartree-Fock calculations [15]. These only range down to ∼20eV and up to ∼400keV for transition metals, which is not nearly infinity. Since the functions die off rapidly as $\int dE/E^2$, the function evaluations are acceptable at the hard x-ray energies available at Beamline 2-1 (∼2keV to 13keV) [16]. Larger concerns are the low sampling rate of the tables, and vast inconsistencies across different published tables like Henke.

Fortunately, the imaginary part $f''(E)$ is experimentally observable because it is proportional to the absorption cross-section from a XANES measurement. This allows us to move back and forth to $f'(E)$, which is easier to fit in SXR because it changes drastically over absorption edges by the number of absorbed electrons [17].

Primarily, K-K transforms are useful for guessing the energy of highest contrast in SXR measurements. A program I implemented, called $kkXANES()$ in Matlab®, takes XANES and transforms it into f' using the first equation above. The energy corresponding to the lowest point in f' was subsequently chosen for resonant SXR scans.

Beyond this application, the K-K relations are powerful as a tool for self-consistent checking of SXR fits: A significant difference between fit parameters and their transforms would indicate unphysical fits. However, FOM is blind to phys-

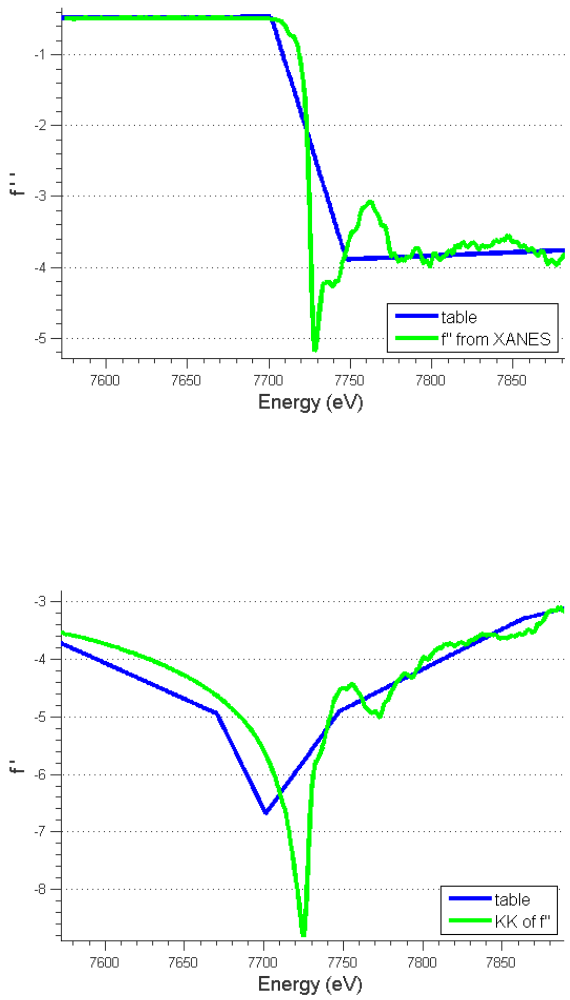

FIG. 7. For sample X11, top: f'', interpreted from XANES, and bottom: its KK Transform, f', compared to table values.

ical or unphysical models, and unlike with SLD plots the appropriate values for f' and f'' are beyond an intuitive human evaluation. Thus, I have implemented code that accomplishes this calculation within the GA, as an objective function separate from the figure of merit, but their successful implementation into the GA will be the subject of future work.

VI. DISCUSSION

The approach to fitting sample X11 was to first support the hypothesis that there are three LSCO layers, with different oxidation states on at least the LSMO interface. From there, I would simultaneously fit all SXR data on the Co edge, to find $f'(E)$, and simply back-transform for each layer to find layer-specific $f''(E)$, which can be interpreted like XANES.

However, the results are inconclusive because, as expected, LSCO is difficult to grow, and the one electron difference between the interfaces and the bulk are too small to fit with significant differences in FOM. I also see an inadequate fit across all energies, suggesting a poor physical model. I suspect a missing layer in our current model, less dense than the LSMO cap, which could be from surface reconstructions or the presence of another chemical constituent. Thus, the first step in this approach is currently under way, and is rapidly approaching a resolution.

VII. CONCLUSION

In summary, I presented a promising method for characterizing the electronic structure of buried interfaces, which cannot be accomplished through other types of measurements. This procedure is complicated for the sample under study, but it may be elaborated upon with a better model, based on a better prediction of the

chemical composition of the sample. Additionally, more advanced fitting algorithms that make full use of the KK relations may help impose more physical solutions. The transform of the fit results to XANES would be an unprecedented feat, which would make the electronic structural characterization understandable to the entire crystallographic community. With this development, materials by design for the permanent magnets in read heads and high-performance magnets would come closer to fruition.

I would like to acknowledge my mentors, Apurva Mehta and Trevor Petach, for their guidance. Special thanks to Kevin Stone, Badri Shayam, and Andre Miranda for their support. This work was supported in part by the U.S. Department of Energy, Office of Science, Office of Workforce Development for Teachers and Scientists (WDTS) under the Science Undergraduate Laboratory Internships Program (SULI).

[1] B. Li, R. V. Chopdekar, E. Arenholz, A. Mehta, and Y. Takamura, Applied Physics Letters **105**, 202401 (2014).

[2] R. Bowley and M. Sánchez, *Introductory statistical mechanics* (Clarendon Press Oxford, 1999).

[3] P. L. Kuhns, M. J. R. Hoch, W. G. Moulton, A. P. Reyes, J. Wu, and C. Leighton, Phys. Rev. Lett. **91**, 127202 (2003).

[4] S. Calvin, *XAFS for Everyone* (CRC Press, 2013).

[5] J. Gazquez, S. Bose, M. Sharma, M. A. Torija, S. J. Pennycook, C. Leighton, and M. Varela, APL Materials **1**, 012105 (2013).

[6] V. K. Malik, C. Hieu Vo, E. Arenholz, A. Scholl, A. T. Young, and Y. Takamura, Journal of Applied Physics **113**, 153907 (2013).

[7] Y. Yoneda, Physical Review **131**, 2010 (1963).

[8] V. Holý, J. Kuběna, I. Ohlída, K. Lischka, and W. Plotz, Phys. Rev. B **47**, 15896 (1993).

[9] V. Holý and T. Baumbach, Phys. Rev. B **49**, 10668 (1994).

[10] S. Sinha, E. B. Sirota, S. Garoff, and H. Stanley, Physical Review B **38**, 2297 (1988).

[11] E. Vlieg and I. Robinson, *Synchrotron Radiation Crystallography*, edited by P. Coppens (Academic Press, London, 1992) Chap. Two-dimensional crystallography, pp. 255–299.

[12] J. Als-Nielsen and D. McMorrow, *Elements of Modern X-ray Physics* (John Wiley and Sons, 2011).

[13] M. Björck and G. Andersson, Journal of Applied Crystallography **40**, 1174 (2007).

[14] V. Lucarini, K.-E. Peiponen, J. J. Saarinen, and E. M. Vartiainen, *Kramers-Kronig Relations in Optical Materials Research*, Springer Series in Optical Sciences, Vol. 110 (Springer, Berlin, 2005).

[15] C. T. Chantler, AIP Conference Proceedings **652**, 370 (2003).

[16] G. Evans and R. F. Pettifer, Journal of Applied Crystallography **34**, 82 (2001).

[17] N. Kemik, M. Gu, F. Yang, C.-Y. Chang, Y. Song, M. Bibee, A. Mehta, M. D. Biegalski, H. M. Christen, N. D. Browning, and Y. Takamura, Applied Physics Letters **99**, 201908 (2011).

VIII. APPENDIX: K-K DERIVATION

Without loss of generality, we may say that electrons have some resonant frequency ω_s and a damping factor Γ, which encapsulates quantum mechanical effects [12]. In the presence of an electric field $E_{in}(t) = \hat{x}E_0e^{i\omega t}$, this yields a displacement per electron

$$x_s(t) = -\frac{e}{m}\frac{E_{in}(t)}{\omega_s^2 - \omega^2 - i\omega\Gamma}$$

where the subscript s is for scatterer. Now consider the radiated electric field, a spherical wave, and evaluate at R for some retarded time $t' = t - R/c$: $E_{rad} = -r_0\ddot{x}(t')E_{in}(t)\frac{e^ikR}{R}$. This is proportional to $E_{in}(t)$ by the atomic scattering length

$$f_s = \frac{\omega^2}{\omega^2 - \omega_s^2 + i\omega\Gamma} \propto \frac{E_{in}(t)}{E_{rad}}$$

so we arrive at a dual definition of $f = \sum_s f_s$, as we defined it before in relation to n.

Since the peaks are at $\omega = \omega_s$ and have $\omega_{FWHM} \approx \Gamma$ which is very small, we approximate the peak from each scatterer as a delta function for convenience. This lets us express what should be $\sum_s$ in integral form. The functions for $f'(E = \hbar\omega)$ and $f''(E = \hbar\omega)$ can be seen to be analytical in the complex plane, since we are discussing a physical system, so we can use transforms to relate them. Before I explicitly noted that for photons $E \propto \omega$ to provide a warning that that they are interchangeable in the literature.

Ralph Kronig and Hendrik Anthony Kramers, derived the Kramers-Kronig (K-K) relations in 1927. They exploited the singularities that develop at the resonant frequencies to employ Cauchy's theorem, rephrasing the problem as a contour integral in the complex plane.

Because the integrands can be shown to go to zero on the infinite radius semi-circle, labeled segment D, and the radius $\epsilon \to 0$ semicircle B, the only nonzero contributions to our contour integral are A and C, which lie along the real axis. The compact form of the relations is one equation:

$$f'(E) + if''(E) = \frac{1}{i\pi}\mathcal{P}\int_{-\infty}^{\infty} \frac{f'(E') + if''(E')}{E' - E}\, dE' \,,$$

where $\mathcal{P}$ denotes a principal integral, to remind us that we must not evaluate exactly at the resonant energy (or frequency) as it is a singularity.

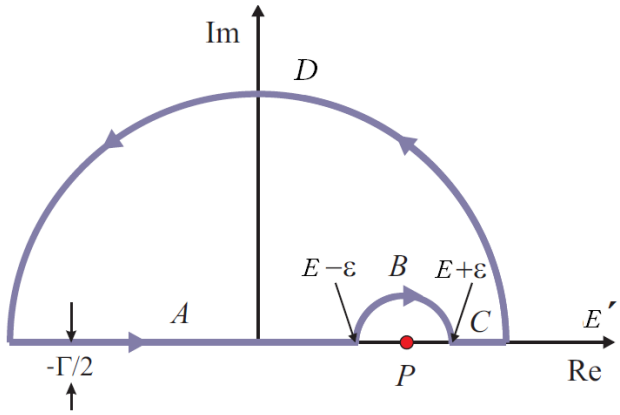

FIG. 8. The contour integral used to find the K-K relations. Adapted from [12].

It can be seen from this that one may equate the real and imaginary parts of both sides to obtain two separate equations. However, energy is confined to positive values, so this form of the relations cannot be evaluated with actual data. Exploiting the symmetry of the functions (f' is even and f'' is odd), integration tricks yield the usable forms:

$$f'(E) = \frac{2}{\pi}\,\mathcal{P}\int_0^\infty \frac{E' f'(E')}{E'^2 - E^2}\,dE'$$

$$f''(E) = -\frac{2E}{\pi}\,\mathcal{P}\int_0^\infty \frac{f'(E')}{E'^2 - E^2}\,dE'$$